Journal Pre-proof

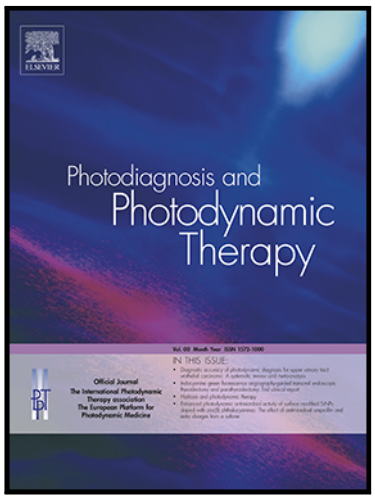

Stage Specific Glaucomatous Changes of the Macula recorded using Spectral Domain Optical Coherence Tomography

Xiao Shang , Jelena Reche , Joel-Benjamin Lincke , Nathanael Urs Häner , Mael Lever , Michael RR Böhm , Caroline Bormann , Martin S Zinkernagel , Jan Darius Unterlauft

PII: S1572-1000(23)00400-3
DOI: https://doi.org/10.1016/j.pdpdt.2023.103673
Reference: PDPDT 103673

To appear in: *Photodiagnosis and Photodynamic Therapy*

Received date: 3 April 2023
Revised date: 18 May 2023
Accepted date: 22 June 2023

Please cite this article as: Xiao Shang , Jelena Reche , Joel-Benjamin Lincke , Nathanael Urs Häner , Mael Lever , Michael RR Böhm , Caroline Bormann , Martin S Zinkernagel , Jan Darius Unterlauft , Stage Specific Glaucomatous Changes of the Macula recorded using Spectral Domain Optical Coherence Tomography, *Photodiagnosis and Photodynamic Therapy* (2023), doi: https://doi.org/10.1016/j.pdpdt.2023.103673

This is a PDF file of an article that has undergone enhancements after acceptance, such as the addition of a cover page and metadata, and formatting for readability, but it is not yet the definitive version of record. This version will undergo additional copyediting, typesetting and review before it is published in its final form, but we are providing this version to give early visibility of the article. Please note that, during the production process, errors may be discovered which could affect the content, and all legal disclaimers that apply to the journal pertain.

© 2023 Published by Elsevier B.V.

source: https://doi.org/10.48350/184232 | downloaded: 29.4.2024

Highlights

- Glaucomatous eyes showed significant thinning of the total retina, ganglion cell layer (GCL), and inner-plexiform layer (IPL) compared to healthy controls in all sectors except the center.
- The thickness of retinal nerve fiber layer (RNFL) was significantly thinner in glaucomatous eyes except in the center, nasal inner, and temporal outer sectors.
- The thinning of layers increased with the severity of glaucoma.
- GCL and IPL thickness demonstrated high ability in discriminating glaucomatous and early-stage glaucomatous eyes from healthy controls.
- Applying the minimal value to the ETDRS grid has the potential to provide a better diagnostic indicator for glaucoma.

Journal Pre-proof

Stage Specific Glaucomatous Changes of the Macula recorded using Spectral Domain Optical Coherence Tomography

Xiao Shang [a], Jelena Reche [a], Joel-Benjamin Lincke [a], Nathanael Urs Häner [a], Mael Lever [b], Michael RR Böhm [b], Caroline Bormann [c], Martin S Zinkernagel [a], and Jan Darius Unterlauft [a,*]

[a] Department of Ophthalmology, Inselspital, Bern University Hospital, University of Bern, Freiburgstrasse 15, 3010, Bern, Switzerland
[b] University Eye Hospital Essen, Hufelandstrasse 55, 45147 Essen, Germany
[c] University Eye Hospital Leipzig, University of Leipzig, Liebigstrasse 10, 04105 Leipzig, Germany
***** Corresponding author: jandarius.unterlauft@insel.ch; Department of Ophthalmology, Inselspital, Bern University Hospital, University of Bern, Freiburgstrasse 15, 3010, Bern, Switzerland.

Journal Pre-proof

Abstract:
Background: This study aimed to compare the thickness of different macular retinal layers in glaucomatous eyes and healthy controls, and evaluate the diagnostic performance of spectral domain optical coherence tomography (SD-OCT) parameters.
Methods: In this cross-sectional comparative study, 48 glaucomatous eyes and 44 healthy controls were included. The thickness of the total retina and all retinal layers were obtained using the Early Treatment Diagnostic Retinopathy Study (ETDRS) grid. The minimal and average values of outer and inner ETDRS-rings were calculated. The diagnostic performance for detection of glaucoma was evaluated using the area under the receiver operating characteristic curve (AUC).
Results: The thickness of the total retina, ganglion cell layer (GCL), and inner-plexiform layer (IPL) was significantly thinner in glaucomatous eyes in all sectors except the center (all $p<0.05$). The thickness of retinal nerve fiber layer (RNFL) was significantly thinner in the glaucoma group except in the center, nasal inner, and temporal outer sectors (all $p<0.05$). Layer thinning advanced with glaucoma severity. The minimal outer GCL thickness showed the highest AUC value for discrimination between glaucomatous eyes and healthy controls(0.955). The minimal outer IPL showed the highest AUC value for discriminating early-stage glaucomatous eyes from healthy controls (0.938).
Conclusions: Glaucomatous eyes were found to have significant thinning in the macular region. GCL and IPL showed high ability to discriminate glaucomatous and early-stage glaucomatous eyes from controls. Applying the minimal value to the ETDRS grid has the potential to provide good diagnostic abilities in glaucoma screening.

Keywords: glaucoma; optical coherence tomography; retinal segmentation; macula

1. Introduction

Globally, glaucoma is amongst the leading causes of blindness with a projected number of 111.8 million people affected by 2040 [1, 2]. In glaucoma, apoptotic demise of retinal ganglion cells (RGC) and their axons leads to increasing visual field scotomas and optic nerve head atrophy. This ultimately leads to ~~complete~~ loss of visual function and blindness if left insufficiently treated [3].

RGC function is usually monitored by perimetry, which is time-consuming, tiring, and heavily dependent on patient collaboration and state of alertness [4]. Monitoring the thickness of the retinal layers including RGC bodies (ganglion cell layer: GCL) or their axons/dendrites (retinal nerve fiber layer: RNFL; inner plexiform layer: IPL) by optical coherence tomography (OCT) is a timesaving complement to perimetry and has found its way into clinical practice and glaucoma management during recent years [5].

Lately, a number of further developments have increased the spatial resolution of OCT measurements and the robustness of automatic retinal layer segmentation algorithms [6]. Modern spectral domain (SD-)OCT has a spatial resolution of 7 µm. Utilizing these techniques, allows physicians to acquire information on single retinal layers in-vivo and tailor individual anti-glaucomatous treatment accordingly.

Glaucoma primarily involves the demise of RGC, located in the three innermost retinal layers (i.e. RNFL, GCL, and IPL) [7]. Judging from preceding OCT studies, atrophy of RGC is mostly restricted to the inner retinal layers in glaucoma [8-10]. Therefore, it was the aim to measure the thickness of total retina and single retinal layers using SD-OCT techniques and to compare results between glaucomatous eyes of different disease stages and healthy controls. The diagnostic ability to differentiate between healthy and glaucomatous eyes was then analyzed.

2. Materials and Methods

This was a cross-sectional, comparative study conducted at the Department of Ophthalmology, Inselspital, Bern, Switzerland. Glaucoma patients and healthy controls were enrolled prospectively. The study adhered to the Tenets of the Declaration of Helsinki and was approved by the Ethics Commission of the Canton of Bern (BASEC-ID. 2021-D0038). Written consent to participate was obtained from all patients prior to inclusion.

Glaucoma diagnosis was verified by slit lamp examination of anterior and posterior eye segments, Goldmann applanation tonometry, standard automated perimetry and SD-OCT recordings of the peripapillary retinal nerve fiber layer (RNFL). Diagnosis was verified by an expert trained in glaucoma subspecialty. In the healthy comparison group, the same diagnostic steps were performed to rule out existing ophthalmologic pathologies that could potentially affect OCT recordings.

For inclusion glaucoma patients had to meet the following criteria: visual acuity had to be <0.3 logMAR (measured using Snellen optotypes transferred into logMAR units for statistical analysis), open anterior chamber angle, regulated intraocular pressure between 10 and 21 mmHg (measured using Goldmann applanation tonometry) with or without application of intraocular pressure (IOP) lowering medication. Visual field was tested using standard automated perimetry (SAP; Octopus, Haag-Streit, Köniz, Switzerland). SAP examination had to be performed within 6 weeks of the OCT measurements and reliability parameters had to be met (<10% of false positives and false negatives). Visual field results were graded using mean deviation (MD) in the following way. For inclusion into early glaucoma group

MD had to lie between 0-5 dB, moderate glaucoma was classified when MD was 5-12 dB and advanced glaucoma was present if MD was >12 dB.

For inclusion into the control group, all signs for any ophthalmic diseases of the anterior and posterior eye segments had to be absent. Visual acuity had to be ≤0.1 logMAR and if necessary the spherical equivalent of the worn spectacles had to lie between -3.0 and +3.0 diopters. SAP had to be without any present scotoma in the central 30°.

OCT measurements were performed using the SPECTRALIS OCT (Heidelberg Engineering, Heidelberg, Germany) using a confocal scanning laser ophthalmoscope obtaining 40,000 A-Scans/minute. For noise reduction active eye-tracking was utilized. Macula and optic nerve head regions were automatically identified by the OCT machine using customary build-in algorithms. The macula region was scanned using 61 parallel running B-scans capturing the central 30° x 30°. To further reduce image noise, repetition rate (ART) for each line scan was set to 26. Scans were aligned to the axis running through the fovea and the center of the optic nerve head. Automated layer segmentation inherent to the OCT device was used and carried out for each recorded B-scan (Figure 1). Individual segments were retinal nerve fiber layer (RNFL), ganglion cell layer (GCL), inner plexiform layer (IPL), inner nuclear layer (INL), outer plexiform layer (OPL), outer nuclear layer (ONL) and retinal pigment epithelium (RPE) layer.

For analysis of the individual retinal layer thickness Early Treatment Diabetic Retinopathy Study (ETDRS) grid was projected on the recorded scans (Figure 1). The ETDRS grid consisted of 9 subfields (central: C; temporal outer and inner: T1 and T2; nasal outer and inner: N1 and N2; inferior outer and inner: I1 and I2; superior outer and inner: S1 and S2). Through automated layer segmentation it was possible to measure mean individual layer thickness for all 9 subfields of the ETDRS grid[11]. The minimal and average values of outer ring (superior outer, inferior outer, nasal outer, and temporal outer) and inner ring (superior inner, inferior inner, nasal inner, and temporal inner) area in each layer were also calculated.

Statistical analysis was performed using SPSS (IBM Version 24.0; Chicago, Illinois, USA) and R (R Core Team (2020). R Foundation for Statistical Computing, Vienna, Austria) software. Patient characteristics, including patient age, BCVA, refraction, visual field indices and retinal layer thickness are given as mean and standard error. The Mann-Whitney-U test and One-way ANOVA test were performed to compare the parameters between groups. Bonferroni correction was applied for multiple testing. The diagnostic ability of each OCT parameter to discriminate glaucomatous eyes and early-stage glaucomatous eyes from healthy controls was investigated using area under the receiver operating characteristics (ROC) curve (AUC) and sensitivity at 90% specificity. An AUC of 1.0 represents perfect discrimination, whereas AUC of 0.5 represents chance discrimination. The Delong method was used to compare the AUCs of the best parameter and the other parameters in each retinal layer [12]. A p-value of less than 0.05 was considered statistical significant.

3. Results

Macula SD-OCT scans were performed in 48 eyes of 48 glaucoma patients (21 female; 27 male) and in 44 eyes of 44 healthy controls (17 female; 27 male). If both eyes of a single glaucoma patient were eligible for inclusion, only data from the worse affected eye (judged from SAP and OCT) were included for further analysis. All measurements were performed between January and May 2022 at the University Eye Hospital Bern, Switzerland. The mean age was 70.8 ±10.8 years (range 37 – 87

years) in the glaucoma group and 65.0 ±13.9 years (range: 37 – 83 years) in the healthy control group. There was no statistically significant difference in gender (p=0.61) and age (p=0.11) between the two groups. The mean BCVA and spherical equivalent for the glaucomatous eyes were 0.11 ±0.21 logMAR and -1.52 ±2.07 D, respectively. The mean deviation (MD) of SAP in the glaucomatous eyes was 9.78±1.09 dB and mean IOP was 13.0 ± 3.6 mmHg. Of the 48 eyes with glaucoma, 20 were in an early stage (MD 0-5 dB), 18 were in a moderate stage (MD 5-12 dB), and the remaining 10 were in an advanced disease stage (MD >12 dB) according to SAP results (see Figure 2 for patient characteristics and stage distribution).

The exact thickness distribution of the total retina in the single ETDRS grid subfields for healthy and glaucoma eyes, as well as for the glaucoma stage-based subgroups, can be found in Table 1 and Figure 3.A. In healthy eyes, the thickness varied between 279 ± 3.5 µm (central sector) and 342 ± 2.4 µm (N2 sector). In the complete group of ~~the~~ glaucoma eyes, the thickness of the total retina varied between 266 ± 2.6 µm (I1 sector) and 327 ± 3.3 µm (N2 sector). While comparing thickness results between the healthy control group and the complete glaucoma group, statistically significant differences were detected for all tested sectors except for the central (Table 1). Further statistical analysis using ANOVA and further pairwise comparison revealed that the differences in thickness distribution were statistically significant depending on glaucoma stage in the S2, I1, N1 and N2 ETDRS sectors (Table 1).

Differences in thickness distribution between healthy and glaucoma eyes were also apparent in the macular RNFL thickness results. As anticipated in both groups, RNFL thickness was lowest in the central ETDRS sector due to the physiological overrepresentation of cone receptors and absence of RGC in the foveola. Apart from this, RNFL thickness ranged between 17.0 ± 0.3 µm (T2) and 47.1 ± 1.2 µm (N1) in the healthy eyes and between 19.4 ± 0.6 µm (T1) and 38.2 ± 1.8 µm (N1) in the complete group of glaucoma eyes. As anticipated, RNFL thickness was highest in the nasal sectors and lowest in the temporal sectors due to the physiological course of RGC axons in the central retina. Further RNFL thickness distribution in the groups of different glaucoma stages is depicted in Figure 3.B and Table 2. Statistical analysis revealed that RNFL thickness differences between healthy and glaucoma eyes was statistically significant in all ETDRS-sectors but the central and T1 sectors (Table 2). Furthermore, differences of RNFL thickness were statistically significant when comparing groups of different glaucoma stages in the S1, S2, I1 and N1 ETDRS sectors (Table 2).

Similarities between the thickness distribution properties in the RNFL and the GCL were apparent. In the group of healthy eyes, GCL thickness ranged from 33.2 ±0.5 µm (I1) and 51.3 ±0.7 µm (I2). In the glaucoma eyes, GCL thickness ranged between 24.1 ±1.0 µm (T1) and 38.9 ±1.4 µm (N2). Thickness differences between healthy and the complete group of glaucoma eyes was again statistically significant for all ETDRS sectors but the central (Table 3). Further statistical analysis also revealed thickness differences of statistical significance between all groups of glaucoma stages for all ETDRS sectors but the central (C) and the N1 sector (see also Table 3 and Figure 3.C).

Thickness distribution characteristics in IPL resemble those already described above for the RNFL and GCL layers. Again when comparing IPL thickness between the glaucoma eyes and the healthy comparison group, differences were of statistical significance for all ETDRS sectors but the central (Table 4). IPL thickness ranged between 27.3 ± 2.8 µm (I1) and 42.5 ± 3.6 µm (N2) in the group of healthy eyes, and

between 22.8 ± 3.5 µm (I1) and 35.5 ± 6.4 µm (N2) in the glaucoma group. As described before for the GCL, further analysis of the thickness distribution of the IPL in the groups of different glaucoma stages using ANOVA returned a statistical significant difference for all ETDRS grid but the C, I2, N2 and T2 sectors (see also Table 4 and Figure 3.D).

The above described differences in thickness distribution between healthy and glaucoma eyes of various disease stages found in the inner retinal layers containing retinal ganglion cells (RNFL, GCL, IPL) and the total retina could not be found in respective analysis of the outer retinal layers (INL, OPL, ONL,RPE). For detailed description, tables and graphics see supplemental material.

The AUC values for the OCT parameters of all sectors in the total retina and inner retinal layers are presented in Table 5. Figure 4 represents the corresponding ROC curves for the OCT parameters with the largest AUC values for discriminating glaucomatous eyes, early-stage glaucomatous eyes and healthy controls. The three best OCT parameters for discriminating between glaucomatous eyes and healthy controls were minimal outer GCL (AUC, 0.955), average outer GCL (AUC, 0.941), and minimal outer IPL (AUC, 0.938). Comparisons between the above parameters showed no significant differences (minimal outer GCL vs average outer GCL: p=0.15, minimal outer GCL vs minimal outer IPL: p=0.45, average outer GCL vs minimal outer IPL: p=0.89). The three best OCT parameters for discriminating between early-stage glaucomatous eyes and healthy controls were minimal outer IPL (AUC, 0.938), I1 IPL (AUC, 0.923), and average outer IPL (AUC, 0.902). The comparisons between the above parameters showed no significant difference (minimal outer IPL vs I1 IPL: p=0.68, minimal outer IPL vs average outer IPL: p=0.07, I1 IPL vs average outer IPL: p=0.59).

Regarding to the location with the largest AUC values in each layer, our analysis revealed that I1 sector had the highest diagnostic ability for discriminating between glaucomatous eyes and healthy controls in the total retina (AUC, 0.825), RNFL (AUC, 0.807), GCL (AUC, 0.937), and IPL (AUC, 0.908). Additionally, the I1 sector also had the largest AUC values for discriminating between early-stage glaucomatous eyes and healthy controls in the total retina (AUC, 0.781), RNFL (AUC, 0.691), GCL (AUC, 0.691), and IPL (AUC, 0.897).

4. Discussion

Glaucoma is a progressive optic neuropathy characterized by degeneration of the dendrites, axons, and cell bodies of RGCs in the retina [13]. It was demonstrated that the macular retinal thickness measurements could be an indicator for RGC loss in glaucomatous eyes [14]. As glaucomatous damage to the macular region can already set in during early disease stages [15], and the macular retinal topography is less variable among individuals than the peripapillary and ONH area topography [16], there has been an increasing number of studies evaluating the application of macular OCT measurements for the diagnosis and monitoring of glaucoma. In the current study, the thickness of the total retina and different macular retinal layers were evaluated and compared between glaucomatous eyes at various disease stages and healthy controls. The diagnostic ability of different retinal layers to help in differentiating between glaucomatous eyes and healthy controls was also investigated.

Using the built-in macular segmentation algorithms of the Spectralis OCT, our investigations show that measurements of the total retina (inner and outer macular rings), RNFL, GCL, and IPL were significantly thinner in glaucomatous eyes than in healthy age-matched controls. As expected, the thickness of the total retina, RNFL,

Journal Pre-proof

GCL, and IPL also gradually decreased in glaucomatous eyes with advancing stages. Our findings are consistent with previous studies reporting significantly lower values in the thickness of the total macular retina, macular ganglion cell-inner plexiform layer (GCIPL, combination of GCL and IPL), and macular ganglion cell complex (GCC, combination of RNFL, GCL, and IPL) ~~measured by OCT in glaucomatous eyes~~ [14, 17-19]. Anatomically, RGCs ~~in the macular region~~ are located in the three inner retinal layers. The axons of RGCs are located in RNFL, the cell bodies of RGCs constitute the majority of the GCL, and the dendrites of RGCs are located in the IPL. Several studies have also shown significant RNFL, GCL, and IPL thinning in eyes suffering from glaucoma [18, 20-23]. These findings suggested separately that RNFL, GCL, and IPL measurements could serve as an effective modality for glaucoma diagnosis and follow-up.

Several previous studies also reported of a high diagnostic ability for combined macular layers like GCIPL [24-28] and GCC [29-31] to discriminate eyes with glaucoma and normal eyes. A much smaller number of studies focused on the diagnostic ability of separate macular retinal layer measurements. The structural glaucomatous damage appeared to be focal in the early stage, then increasingly diffuse in the advanced stage. Therefore, we added additional parameters to our analysis, such as the minimal and average values of outer and inner rings of the ETDRS grid of each macular layer.

The current study demonstrated that the minimal outer GCL (AUC, 0.955), average outer GCL (AUC, 0.941), and minimal outer IPL (AUC, 0.938) showed the best diagnostic ability to discriminate between glaucomatous eyes and healthy controls. However, we found no significant difference among the diagnostic performances of these three parameters. Kim et al [23] using the same Spectralis SD-OCT also reported similar diagnostic performances of separate macular layer measurements, but slightly higher AUC values for RNFL measurements. This could be due to the different scan areas (8x8 posterior pole grid) and sectioning methods utilized. Also, their study population consisted exclusively of persons of Korean descent that were already reported to have a different RNFL distribution than Caucasians and also a larger percentage of angle closure glaucoma than in our Caucasian patient population solely suffering of primary open-angle glaucoma [32, 33]. The minimal outer IPL (AUC, 0.938), inferior outer IPL (AUC, 0.923), and average outer IPL (AUC, 0.902) were the OCT parameters with the best performance for discrimination of early-stage glaucomatous eyes and healthy controls. These three parameters showed no~~w~~ significant difference in diagnostic performance. This seems to be consistent with prior findings reporting that the disruption of RGC dendrites may precede histological changes of the axon and soma of RGCs in an animal glaucoma model [34, 35]. Our findings may suggest the potential for application of the minimal and average values of the outer rings of the ETDRS grids for individual layer measurement, such as GCL and IPL, to aid in the early diagnosis of glaucoma.

As for the OCT parameters derived from the regular Spectralis SD-OCT reports, the inferior outer sector showed the best diagnostic ability in the total retina, RNFL, GCL, and IPL for differentiating glaucomatous eyes and healthy controls. Notably, similar results were also observed by Pazos et al [18] who evaluated the diagnostic accuracy of different macular layers, and reported the most fitting RNFL sector to be the inferior outer. Chien et al [36] compared the glaucoma diagnostic ability of macular layer OCT parameters in different scan sizes (3-, 3.45-, and 6-mm grid) and also observed that the inferior outer region had the best AUC in both RNFL and GCC.

Journal Pre-proof

These findings confirmed that larger macular grids could improve the diagnostic ability in glaucoma, and suggested that the inferior outer sector could be more vulnerable to glaucomatous damage.

There were a number of limitations to this study. First, the sample size in this study was comparably small for each glaucoma stage. This was especially so for the group of advanced glaucoma eyes. Additionally, the cross-sectional design of this study could not reveal the temporal relationship of damage in different retinal layers. Future prospective, longitudinal studies with larger sample sizes are needed to evaluate the temporal relationship of glaucomatous damage in different retinal layers and locations. Second, this study did not include the measurements of axial length, which is considered as a confounding factor for OCT measurements [37]. However, in order to minimize the effect of individual differences in axial length on the diagnostic ability of OCT measurements, we only included subjects within a spherical equivalent range of -3.0 D to +3.0 D. Another limitation of the current study was the inability to investigate the retinal thickness outside the 6-mm diameter ETDRS grid.

5. Conclusions

In conclusion, we could demonstrate that the thickness of the total retina, RNFL, GCL, and IPL are reduced with advancing stages of glaucoma severity. The macular GCL and IPL showed high diagnostic ability in discriminating between glaucomatous eyes and early-stage glaucomatous eyes and healthy eyes separately. Our findings support the use of GCL and IPL thickness measurements for early glaucoma detection using SD-OCT. Moreover, we suggest that the minimal and average values of the outer ring sections in each layer could be a better modality for glaucoma diagnosis than routine measurements.

References

1. Steinmetz, J.D.; Bourne, R.R.; Briant, P.S.; Flaxman, S.R.; Taylor, H.R.; Jonas, J.B.; Abdoli, A.A.; Abrha, W.A.; Abualhasan, A.; Abu-Gharbieh, E.G. Causes of blindness and vision impairment in 2020 and trends over 30 years, and prevalence of avoidable blindness in relation to VISION 2020: the Right to Sight: an analysis for the Global Burden of Disease Study. *The Lancet Global Health* **2021**, *9*, e144-e160, doi: 10.1016/S2214-109X(20)30489-7.
2. Tham, Y.-C.; Li, X.; Wong, T.Y.; Quigley, H.A.; Aung, T.; Cheng, C.-Y. Global prevalence of glaucoma and projections of glaucoma burden through 2040: a systematic review and meta-analysis. *Ophthalmology* **2014**, *121*, 2081-2090, doi: 10.1016/j.ophtha.2014.05.013.
3. Weinreb, R.N.; Leung, C.K.; Crowston, J.G.; Medeiros, F.A.; Friedman, D.S.; Wiggs, J.L.; Martin, K.R. Primary open-angle glaucoma. *Nature reviews Disease primers* **2016**, *2*, 1-19, doi: 10.1038/nrdp.2016.67.
4. Heijl, A.; Åsman, P. Pitfalls of automated perimetry in glaucoma diagnosis: Editorial review. *Current opinion in ophthalmology* **1995**, *6*, 46-51, doi: 10.1097/00055735-199504000-00008.
5. Hood, D.C.; La Bruna, S.; Tsamis, E.; Thakoor, K.A.; Rai, A.; Leshno, A.; de Moraes, C.G.; Cioffi, G.A.; Liebmann, J.M. Detecting glaucoma with only OCT: Implications for the clinic, research, screening, and AI development. *Progress in Retinal and Eye Research* **2022**, 101052, doi: 10.1016/j.preteyeres.2022.101052.
6. Vazquez, L.E.; Bye, A.; Aref, A.A. Recent developments in the use of optical coherence tomography for glaucoma. *Current opinion in ophthalmology* **2021**, *32*, 98-104, doi: 10.1097/ICU.0000000000000733.

7. De Moraes, C.G. Anatomy of the visual pathways. *Journal of glaucoma* **2013**, *22*, S2-S7, doi: 10.1097/IJG.0b013e3182934978..
8. Nouri-Mahdavi, K.; Weiss, R.E. Detection of glaucoma deterioration in the macular region with optical coherence tomography: challenges and solutions. *American Journal of Ophthalmology* **2021**, *222*, 277-284, doi: 10.1016/j.ajo.2020.09.026.
9. Lever, M.; Glaser, M.; Chen, Y.; Halfwassen, C.; Unterlauft, J.D.; Bechrakis, N.E.; Böhm, M.R. Microvascular and Structural Alterations of the Macula in Early to Moderate Glaucoma: An Optical Coherence Tomography-Angiography Study. *Journal of clinical medicine* **2021**, *10*, 5017, doi: 10.3390/jcm10215017.
10. Lever, M.; Halfwassen, C.; Unterlauft, J.D.; Bechrakis, N.E.; Manthey, A.; Böhm, M.R. The Paediatric glaucoma diagnostic ability of optical coherence tomography: a comparison of macular segmentation and peripapillary retinal nerve fibre layer thickness. *Biology* **2021**, *10*, 260, doi: 10.3390/biology10040260.
11. Group, E.T.D.R.S.R. Grading diabetic retinopathy from stereoscopic color fundus photographs—an extension of the modified Airlie House classification: ETDRS report number 10. *Ophthalmology* **1991**, *98*, 786-806.
12. DeLong, E.R.; DeLong, D.M.; Clarke-Pearson, D.L. Comparing the areas under two or more correlated receiver operating characteristic curves: a nonparametric approach. *Biometrics* **1988**, 837-845.
13. Morrison, J.C.; Guo, W.O.C.Y.; Johnson, E.C. Pathophysiology of human glaucomatous optic nerve damage: insights from rodent models of glaucoma. *Experimental eye research* **2011**, *93*, 156-164, doi: 10.1016/j.exer.2010.08.005.
14. Greenfield, D.S.; Bagga, H.; Knighton, R.W. Macular thickness changes in glaucomatous optic neuropathy detected using optical coherence tomography. *Archives of Ophthalmology* **2003**, *121*, 41-46, doi: 10.1001/archopht.121.1.41.
15. Hood, D.C.; Raza, A.S.; de Moraes, C.G.V.; Liebmann, J.M.; Ritch, R. Glaucomatous damage of the macula. *Progress in retinal and eye research* **2013**, *32*, 1-21, doi: 10.1016/j.preteyeres.2012.08.003.
16. Curcio, C.A.; Allen, K.A. Topography of ganglion cells in human retina. *Journal of comparative Neurology* **1990**, *300*, 5-25, doi: 10.1002/cne.903000103.
17. Mwanza, J.-C.; Budenz, D.L.; Godfrey, D.G.; Neelakantan, A.; Sayyad, F.E.; Chang, R.T.; Lee, R.K. Diagnostic performance of optical coherence tomography ganglion cell–inner plexiform layer thickness measurements in early glaucoma. *Ophthalmology* **2014**, *121*, 849-854, doi: 10.1016/j.ophtha.2013.10.044.
18. Pazos, M.; Dyrda, A.A.; Biarnés, M.; Gómez, A.; Martín, C.; Mora, C.; Fatti, G.; Antón, A. Diagnostic accuracy of spectralis SD OCT automated macular layers segmentation to discriminate normal from early glaucomatous eyes. *Ophthalmology* **2017**, *124*, 1218-1228, doi: 10.1016/j.ophtha.2017.03.044.
19. Tanito, M.; Itai, N.; Ohira, A.; Chihara, E. Reduction of posterior pole retinal thickness in glaucoma detected using the Retinal Thickness Analyzer. *Ophthalmology* **2004**, *111*, 265-275, doi: 10.1016/j.ophtha.2003.05.023.
20. Tan, O.; Li, G.; Lu, A.T.-H.; Varma, R.; Huang, D.; Group, A.I.f.G.S. Mapping of macular substructures with optical coherence tomography for glaucoma

Journal Pre-proof

diagnosis. *Ophthalmology* **2008**, *115*, 949-956, doi: 10.1016/j.ophtha.2007.08.011.
21. de A Moura, A.; Raza, A.; Lazow, M.; De Moraes, C.; Hood, D. Retinal ganglion cell and inner plexiform layer thickness measurements in regions of severe visual field sensitivity loss in patients with glaucoma. *Eye* **2012**, *26*, 1188-1193, doi: 10.1038/eye.2012.110.
22. Kim, H.J.; Lee, S.-Y.; Park, K.H.; Kim, D.M.; Jeoung, J.W. Glaucoma diagnostic ability of layer-by-layer segmented ganglion cell complex by spectral-domain optical coherence tomography. *Investigative ophthalmology & visual science* **2016**, *57*, 4799-4805, doi: 10.1167/iovs.16-19214.
23. Kim, E.K.; Park, H.-Y.L.; Park, C.K. Segmented inner plexiform layer thickness as a potential biomarker to evaluate open-angle glaucoma: Dendritic degeneration of retinal ganglion cell. *PloS one* **2017**, *12*, e0182404, doi: 10.1371/journal.pone.0182404.
24. Begum, V.U.; Addepalli, U.K.; Yadav, R.K.; Shankar, K.; Senthil, S.; Garudadri, C.S.; Rao, H.L. Ganglion cell-inner plexiform layer thickness of high definition optical coherence tomography in perimetric and preperimetric glaucoma. *Investigative ophthalmology & visual science* **2014**, *55*, 4768-4775, doi: 10.1167/iovs.14-14598.
25. Mwanza, J.-C.; Durbin, M.K.; Budenz, D.L.; Sayyad, F.E.; Chang, R.T.; Neelakantan, A.; Godfrey, D.G.; Carter, R.; Crandall, A.S. Glaucoma diagnostic accuracy of ganglion cell–inner plexiform layer thickness: comparison with nerve fiber layer and optic nerve head. *Ophthalmology* **2012**, *119*, 1151-1158, doi: 10.1016/j.ophtha.2011.12.014.
26. Kim, M.J.; Jeoung, J.W.; Park, K.H.; Choi, Y.J.; Kim, D.M. Topographic profiles of retinal nerve fiber layer defects affect the diagnostic performance of macular scans in preperimetric glaucoma. *Investigative Ophthalmology & Visual Science* **2014**, *55*, 2079-2087, doi: 10.1167/iovs.13-13506.
27. Choi, Y.J.; Jeoung, J.W.; Park, K.H.; Kim, D.M. Glaucoma detection ability of ganglion cell-inner plexiform layer thickness by spectral-domain optical coherence tomography in high myopia. *Investigative ophthalmology & visual science* **2013**, *54*, 2296-2304, doi: 10.1167/iovs.12-10530.
28. Shin, H.-Y.; Park, H.-Y.L.; Jung, K.-I.; Choi, J.-A.; Park, C.K. Glaucoma diagnostic ability of ganglion cell–inner plexiform layer thickness differs according to the location of visual field loss. *Ophthalmology* **2014**, *121*, 93-99, doi: 10.1016/j.ophtha.2013.06.041.
29. Seong, M.; Sung, K.R.; Choi, E.H.; Kang, S.Y.; Cho, J.W.; Um, T.W.; Kim, Y.J.; Park, S.B.; Hong, H.E.; Kook, M.S. Macular and peripapillary retinal nerve fiber layer measurements by spectral domain optical coherence tomography in normal-tension glaucoma. *Investigative ophthalmology & visual science* **2010**, *51*, 1446-1452, doi: 10.1167/iovs.09-4258.
30. Arintawati, P.; Sone, T.; Akita, T.; Tanaka, J.; Kiuchi, Y. The applicability of ganglion cell complex parameters determined from SD-OCT images to detect glaucomatous eyes. *Journal of glaucoma* **2013**, *22*, 713-718, doi: 10.1097/IJG.0b013e318259b2e1.
31. Teixeira, I.C.; Bresciani-Battilana, E.; Barbosa, D.T.; Caixeta-Umbelino, C.; Paolera, M.D.; Kasahara, N. Correlation between the ganglion cell complex and functional measures in glaucoma patients and suspects. *International ophthalmology* **2015**, *35*, 81-87.

Journal Pre-proof

32. Alasil, T.; Wang, K.; Keane, P.A.; Lee, H.; Baniasadi, N.; de Boer, J.F.; Chen, T.C. Analysis of normal retinal nerve fiber layer thickness by age, sex, and race using spectral domain optical coherence tomography. *Journal of glaucoma* **2013**, *22*, 532-541, doi: 10.1097/IJG.0b013e318255bb4a.
33. O'Rese, J.K.; Girkin, C.A.; Budenz, D.L.; Durbin, M.K.; Feuer, W.J.; Group, C.O.N.D.S. Effect of race, age, and axial length on optic nerve head parameters and retinal nerve fiber layer thickness measured by Cirrus HD-OCT. *Archives of ophthalmology* **2012**, *130*, 312-318, doi: 10.1001/archopthalmol.2011.1576.
34. Frankfort, B.J.; Khan, A.K.; Dennis, Y.T.; Chung, I.; Pang, J.-J.; Yang, Z.; Gross, R.L.; Wu, S.M. Elevated intraocular pressure causes inner retinal dysfunction before cell loss in a mouse model of experimental glaucoma. *Investigative ophthalmology & visual science* **2013**, *54*, 762-770, doi: 10.1167/iovs.12-10581.
35. El-Danaf, R.; Huberman, A. Characteristic patterns of dendritic remodeling in early-stage glaucoma: evidence from genetically identified retinal ganglion cell types. *The Journal of neuroscience : the official journal of the Society for Neuroscience* **2015**, *35*, 2329-2343, doi:10.1523/jneurosci.1419-14.2015.
36. Chien, J.; Ghassibi, M.; Patthanathamrongkasem, T.; Abumasmah, R.; Rosman, M.; Skaat, A.; Tello, C.; Liebmann, J.; Ritch, R.; Park, S. Glaucoma Diagnostic Capability of Global and Regional Measurements of Isolated Ganglion Cell Layer and Inner Plexiform Layer. *Journal of glaucoma* **2017**, *26*, 208-215, doi:10.1097/ijg.0000000000000572.
37. Liu, X.; Shen, M.; Yuan, Y.; Huang, S.; Zhu, D.; Ma, Q.; Ye, X.; Lu, F. Macular Thickness Profiles of Intraretinal Layers in Myopia Evaluated by Ultrahigh-Resolution Optical Coherence Tomography. *American journal of ophthalmology* **2015**, *160*, 53-61.e52, doi:10.1016/j.ajo.2015.03.012.

Journal Pre-proof

Table 1: Mean thickness of the total retina in the single ETDRS grid sectors measured using SD-OCT in eyes of different glaucoma stages and healthy controls.

Retina	C	S1	S2	I1	I2	N1	N2	T1	T2
healthy	279±3.5 (238-346)	296±2.5 (267-338)	339±2.5 (306-383)	287±2.4 (264-334)	338±2.4 (308-373)	311±2.6 (278-388)	342±2.4 (314-386)	281±2.7 (247-334)	326±2.6 (292-367)
all glaucoma	282±5.2 (237-373)	280±4.9 (240-332)	323±5.1 (265-387)	266±2.6 (224-310)	315±3.4 (259-372)	290±2.5 (253-327)	327±3.3 (278-379)	268±3.0 (235-331)	312±4.2 (268-392)
p[a]	0.87	**<0.001**	**<0.001**	**<0.001**	**<0.001**	**<0.001**	**<0.001**	**<0.001**	**<0.001**
early	277±3.7 (237-302)	282±3.1 (259-316)	332±3.6 (307-369)	272±2.3 (255-289)	322±3.1 (296-344)	299±2.7 (275-320)	337±3.8 (312-371)	270±2.6 (251-287)	317±3.6 (295-341)
moderate	278±7.3 (251-367)	271±5.7 (240-332)	312±6.5 (265-385)	257±5.0 (224-310)	307±6.1 (259-363)	286±4.5 (254-322)	322±5.4 (278-377)	264±6.1 (235-323)	303±6.1 (268-367)
advanced	285±13.6 (246-373)	272±8.0 (248-328)	310±10.3 (274-387)	266±6.6 (235-306)	311±8.9 (275-372)	283±6.5 (253-327)	315±9.0 (279-379)	269±8.5 (244-331)	307±11.4 (278-392)
p[b]	0.78	0.23	**0.02**	**0.04**	0.12	**0.02**	**0.02**	0.65	0.22
P1[c]	1.00	0.35	**0.04**	**0.04**	0.15	0.06	0.12	1.00	0.27
P2[c]	1.00	0.62	0.09	1.00	0.58	0.05	**0.04**	1.00	0.88
P3[c]	1.00	1.00	1.00	0.60	1.00	1.00	1.00	1.00	1.00

Data are expressed as mean ± standard error (minimum-maximum).

[a] Mann-Whitney U test.

[b] One-way ANOVA test.

[c] One-way ANOVA test post hoc Bonferroni test. P1: pairwise comparison between early and moderate glaucoma group; P2: pairwise comparison between early and advanced glaucoma group; P3: pairwise comparison between moderate and advanced glaucoma group.

ETDRS, Early Treatment Diabetic Retinopathy Study; SD-OCT, spectral-domain optic coherence tomography; C, center sector; S1, superior outer sector; S2, superior inner sector; I1, inferior outer sector; I2, inferior inner sector; N1, nasal outer sector; N2, nasal inner sector; T1, temporal outer sector; T2, temporal inner sector; p values less than 0.05 are in bold.

Table 2: Mean thickness of the retinal nerve fiber layer in the single ETDRS grid sectors measured using SD-OCT in eyes of different glaucoma stages and healthy controls.

RNFL	C	S1	S2	I1	I2	N1	N2	T1	T2
Healthy	13.2±0.4 (9-22)	36.7±0.8 (29-48)	24.1±0.5 (15-35)	38.5±0.7 (30-46)	24.7±0.5 (18-33)	47.1±1.2 (16-65)	20.6±0.4 (16-26)	18.9±0.7 (15-46)	17.0±0.3 (12-21)
all glaucoma	13.5±0.8 (6-28)	30.5±1.1 (16-54)	24.6±1.8 (13-51)	28.1±1.4 (16-59)	21.6±0.9 (13-41)	38.2±1.8 (17-71)	21.0±0.7 (13-36)	19.4±0.6 (15-38)	19.5±1.2 (13-44)
p[a]	0.19	**<0.001**	**<0.001**	**<0.001**	**<0.001**	**<0.001**	0.62	0.55	**<0.01**
Early	12.9±0.5 (8-18)	33.8±2.0 (20-54)	24.8±1.1 (18-35)	33.8±2.5 (17-59)	23.2±1.3 (13-36)	44.3±3.0 (19-71)	22.0±0.9 (15-32)	19.6±1.1 (16-38)	18.3±0.5 (15-24)
moderate	13.6±1.0 (10-28)	27.3±1.9 (17-41)	21.5±1.9 (16-51)	25.3±2.1 (17-44)	21.9±1.7 (13-41)	37.4±2.5 (21-59)	21.2±1.2 (15-36)	19.2±0.9 (15-30)	19.9±1.5 (15-44)
advanced	11.6±1.4 (6-20)	22.2±1.3 (16-29)	17.5±1.6 (13-30)	23.8±2.1 (16-41)	17.7±1.0 (13-22)	29.4±2.2 (17-36)	17.9±1.5 (13-28)	19.0±0.7 (16-24)	17.0±0.7 (13-21)
p[b]	0.41	**<0.001**	**0.02**	**0.008**	0.06	**0.006**	0.09	0.94	0.22
P1[c]	1.00	0.05	0.35	**0.03**	1.00	0.22	1.00	1.00	0.73
P2[c]	1.00	**0.002**	**0.01**	**0.03**	0.06	**0.005**	0.09	1.00	1.00
P3[c]	0.55	0.33	0.33	1.00	0.23	0.24	0.24	1.00	0.28

Data are expressed as mean ± standard error (minimum-maximum).

[a] Mann-Whitney U test.

[b] One-way ANOVA test.

Journal Pre-proof

[c] One-way ANOVA test post hoc Bonferroni test. P1: pairwise comparison between early and moderate glaucoma group; P2: pairwise comparison between early and advanced glaucoma group; P3: pairwise comparison between moderate and advanced glaucoma group.

ETDRS, Early Treatment Diabetic Retinopathy Study; SD-OCT, spectral-domain optic coherence tomography; RNFL, retinal nerve fiber layer; C, center sector; S1, superior outer sector; S2, superior inner sector; I1, inferior outer sector; I2, inferior inner sector; N1, nasal outer sector; N2, nasal inner sector; T1, temporal outer sector; T2, temporal inner sector; p values less than 0.05 are in bold.

Table 3: Mean thickness of the ganglion cell layer in the single ETDRS grid sectors measured using SD-OCT in eyes of different glaucoma stages and healthy controls.

GCL	C	S1	S2	I1	I2	N1	N2	T1	T2
healthy	17.1±0.9 (9-35)	33.7±0.5 (27-42)	51.2±0.7 (40-61)	33.2±0.5 (27-42)	51.3±0.7 (40-60)	36.8±0.6 (28-45)	50.6±0.8 (41-63)	34.7±0.6 (28-45)	46.6±0.9 (36-58)
all glaucoma	15.0±1.1 (7-44)	26.2±0.8 (12-34)	38.5±1.4 (8-59)	24.9±0.7 (14-35)	35.9±1.6 (13-55)	29.0±0.7 (19-45)	38.9±1.4 (20-57)	24.1±1.0 (14-45)	32.5±1.6 (16-70)
p[a]	0.06	**<0.001**	**<0.001**	**<0.001**	**<0.001**	**<0.001**	**<0.001**	**<0.001**	**<0.001**
early	15.1±0.8 (9-20)	28.5±0.9 (20-34)	45.8±1.2 (35-56)	27.4±0.9 (17-32)	40.7±2.5 (14-54)	30.8±0.8 (24-37)	44.3±2.2 (21-57)	28.1±1.4 (16-39)	38.6±2.0 (21-50)
moderate	14.3±0.8 (9-21)	24.6±0.9 (19-31)	34.0±1.4 (23-42)	22.3±1.0 (14-30)	32.9±2.2 (13-47)	27.6±0.9 (22-35)	36.5±1.9 (20-49)	20.2±1.0 (14-29)	26.8±1.6 (18-44)
advanced	16.3±3.7 (7-44)	24.4±1.9 (12-32)	32.0±4.4 (8-59)	24.5±1.6 (18-35)	31.6±3.4 (19-55)	27.9±2.4 (19-45)	32.6±3.1 (20-49)	23.4±2.8 (14-45)	30.4±4.9 (16-70)
p[b]	0.71	**0.01**	**<0.001**	**0.003**	**0.03**	0.09	**0.003**	**0.001**	**0.002**
P1[c]	1.00	**0.02**	**<0.001**	**0.002**	0.08	0.13	**0.04**	**0.001**	**0.002**
P2[c]	1.00	0.05	**<0.001**	0.28	0.09	0.36	**0.006**	0.17	0.12
P3[c]	1.00	1.00	1.00	0.62	1.00	1.00	0.85	0.57	1.00

Data are expressed as mean ± standard error (minimum-maximum).

[a] Mann-Whitney U test.

[b] One-way ANOVA test.

[c] One-way ANOVA test post hoc Bonferroni test. P1: pairwise comparison between early and moderate glaucoma group; P2: pairwise comparison between early and advanced glaucoma group; P3: pairwise comparison between moderate and advanced glaucoma group.

ETDRS, Early Treatment Diabetic Retinopathy Study; SD-OCT, spectral-domain optic coherence tomography; GCL, ganglion cell layer; C, center sector; S1, superior outer sector; S2, superior inner sector; I1, inferior outer sector; I2, inferior inner sector; N1, nasal outer sector; N2, nasal inner sector; T1, temporal outer sector; T2, temporal inner sector; p values less than 0.05 are in bold.

Table 4: Mean thickness of the inner plexiform layer in the single ETDRS grid sectors measured using SD-OCT in eyes of different glaucoma stages and healthy controls.

IPL	C	S1	S2	I1	I2	N1	N2	T1	T2
healthy	22.9±4.9 (17-36)	28.1±2.7 (23-34)	40.8±3.5 (31-49)	27.3±2.8 (22-37)	41.5±3.3 (35-49)	28.5±3.2 (21-37)	42.5±3.6 (36-52)	31.3±2.7 (26-41)	41.1±3.9 (32-51)
all glaucoma	21.1±5.0 (14-45)	23.7±3.9 (15-39)	33.3±6.7 (17-55)	22.8±3.5 (17-40)	32.1±7.6 (19-64)	23.7±3.7 (18-40)	35.5±6.4 (22-49)	26.4±5.1 (19-50)	33.5±7.5 (22-63)
p[a]	0.06	**<0.001**	**<0.001**	**<0.001**	**<0.001**	**<0.001**	**<0.001**	**<0.001**	**<0.001**
early	21.9±0.7 (16-26)	24.1±0.6 (19-27)	36.8±0.8 (29-41)	22.8± 0.5 (19-28)	34.3±1.4 (22-42)	24.5±0.5 (21-29)	38.1±1.3 (26-47)	27.5±0.7 (22-34)	36.4±1.3 (24-47)
moderate	20.3±0.8 (15-30)	21.9±0.8 (15-28)	30.2±1.0 (25-39)	21.4±0.6 (17-26)	29.6±1.3 (19-40)	22.1±0.7 (18-27)	34.1±1.2 (22-46)	23.9±0.8 (19-33)	30.8±1.3 (22-44)
advanced	20.9±2.9 (14-45)	26.0±1.7 (21-39)	31.9±3.6 (17-55)	25.5±1.7 (22-40)	32.1±3.8 (22-64)	25.1±1.9 (19-40)	33.0±2.7 (22-49)	28.7±2.6 (21-50)	32.7±3.6 (24-63)

Journal Pre-proof

p[b]	0.65	**0.02**	**0.005**	**0.009**	0.17	**0.04**	0.06	**0.02**	0.06
P1[c]	1.00	0.25	**0.005**	0.60	0.18	0.11	0.16	0.08	0.06
P2[c]	1.00	0.52	0.13	0.10	1.00	1.00	0.12	1.00	0.57
P3[c]	1.00	**0.02**	1.00	**0.007**	1.00	0.10	1.00	0.05	1.00

Data are expressed as mean ± standard error (minimum-maximum).

[a] Mann-Whitney U test.

[b] One-way ANOVA test.

[c] One-way ANOVA test post hoc Bonferroni test. P1: pairwise comparison between early and moderate glaucoma group; P2: pairwise comparison between early and advanced glaucoma group; P3: pairwise comparison between moderate and advanced glaucoma group.

ETDRS, Early Treatment Diabetic Retinopathy Study; SD-OCT, spectral-domain optic coherence tomography; IPL, inner-plexiform layer; C, center sector; S1, superior outer sector; S2, superior inner sector; I1, inferior outer sector; I2, inferior inner sector; N1, nasal outer sector; N2, nasal inner sector; T1, temporal outer sector; T2, temporal inner sector; p values less than 0.05 are in bold.

Journal Pre-proof

Table 5. Diagnostic Abilities for Glaucoma and Early Glaucoma of OCT parameters in each retinal layer. Sensitivity at 90% specificity of each OCT parameter is presented as percentages. P-values indicate the comparison between the OCT parameters with the largest AUC values and other OCT parameters in each retinal layer. P-values less than 0.05 are in bold.

		Normal Control vs Glaucoma			Normal Control vs Early-stage Glaucoma		
Sublayer	**Location**	**AUC (95%CI)**	**Sensitivity at 90% Specificity**	**P value[a]**	**AUC (95%CI)**	**Sensitivity at 90% Specificity**	**P value[a]**
Total Retina	Center	0.510 (0.389-0.630)	14.2	**<0.001**	0.456 (0.304-0.607)	15.0	**<0.001**
	S1	0.790 (0.697-0.883)	59.2	0.37	0.734 (0.602-0.865)	42.0	0.42
	S2	0.752 (0.651-0.854)	60.4	0.05	0.613 (0.463-0.764)	30.0	**0.006**
	I1	0.826 (0.741-0.910)	56.3	Ref	0.781 (0.665-0.896)	35.0	Ref
	I2	0.809 (0.720-0.899)	57.9	0.59	0.760 (0.634-0.886)	38.0	0.67
	N1	0.785 (0.693-0.877)	52.9	0.27	0.694 (0.559-0.828)	27.0	0.13
	N2	0.729 (0.624-0.834)	53.5	**0.04**	0.590 (0.428-0.753)	38.5	**0.02**
	T1	0.725 (0.621-0.830)	50.8	**0.004**	0.686 (0.551-0.822)	37.0	0.08
	T2	0.742 (0.637-0.846)	60.4	**0.02**	0.633 (0.477-0.789)	45.0	**0.02**
	Average Outer	0.800 (0.710-0.889)	57.1	0.25	0.745 (0.620-0.870)	37.0	0.38
	Minimal Outer	0.798 (0.708-0.887)	55.0	0.28	0.728 (0.603-0.854)	37.0	0.16
	Average Inner	0.765 (0.663-0.866)	58.3	0.10	0.670 (0.520-0.820)	35.0	0.08
	Minimal Inner	0.771 (0.671-0.870)	65.4	0.14	0.670 (0.519-0.822)	45.0	0.08
RNFL	Center	0.579 (0.460-0.698)	19.0	**0.001**	0.520 (0.358-0.683)	13.5	0.10
	S1	0.774 (0.675-0.873)	62.5	0.43	0.624 (0.455-0.794)	40.0	0.33
	S2	0.683 (0.571-0.794)	41.3	**0.02**	0.498 (0.335-0.661)	12.0	**0.03**
	I1	0.807 (0.709-0.905)	72.0	Ref	0.691 (0.511-0.871)	57.8	Ref
	I2	0.732 (0.627-0.837)	48.8	0.05	0.607 (0.441-0.773)	35.0	0.13
	N1	0.732 (0.625-0.838)	61.3	**0.04**	0.591 (0.424-0.759)	37.0	0.06
	N2	0.530 (0.410-0.650)	22.1	**<0.001**	0.427 (0.264-0.589)	10.0	**<0.001**
	T1	0.465 (0.346-0.583)	10.6	**<0.001**	0.489 (0.327-0.651)	13.6	**0.02**
	T2	0.336 (0.224-0.448)	10.4	**<0.001**	0.320 (0.167-0.473)	8.0	**<0.001**
	Average Outer	0.781 (0.681-0.882)	62.5	0.25	0.640 (0.468-0.813)	40.0	0.17
	Minimal Outer	0.478 (0.359-0.596)	10.3	**<0.001**	0.484 (0.325-0.643)	11.3	**0.008**
	Average Inner	0.652 (0.537-0.766)	42.5	**0.001**	0.513 (0.344-0.681)	20.7	**0.009**
	Minimal Inner	0.464 (0.342-0.585)	22.1	**<0.001**	0.338 (0.174-0.502)	13.0	**<0.001**
GCL	Center	0.612 (0.497-0.727)	30.0	**<0.001**	0.560 (0.411-0.708)	21.4	**<0.001**
	S1	0.905 (0.848-0.962)	73.3	**0.006**	0.844 (0.745-0.942)	60.4	0.17
	S2	0.880 (0.810-0.951)	75.0	**0.004**	0.773 (0.652-0.895)	45.0	**0.01**
	I1	0.937 (0.889-0.984)	85.7	0.33	0.897 (0.819-0.974)	75.3	Ref
	I2	0.901 (0.838-0.963)	74.6	**0.02**	0.824 (0.714-0.934)	53.0	0.11
	N1	0.904 (0.842-0.967)	71.5	0.08	0.881 (0.797-0.965)	59.3	0.70
	N2	0.836 (0.754-0.918)	64.0	**<0.001**	0.683 (0.534-0.832)	35.0	**0.002**
	T1	0.899 (0.828-0.970)	80.8	**0.03**	0.816 (0.687-0.945)	62.0	0.12
	T2	0.864 (0.787-0.941)	70.8	**0.002**	0.745 (0.611-0.879)	40.0	**0.007**
	Average Outer	0.941 (0.897-0.984)	82.9	0.15	0.882 (0.797-0.968)	67.0	0.64
	Minimal Outer	0.955 (0.918-0.993)	85.8	Ref	0.894 (0.813-0.976)	66.0	0.93
	Average Inner	0.883 (0.810-0.955)	75.0	**0.005**	0.774 (0.642-0.905)	50.0	**0.02**
	Minimal Inner	0.866 (0.790-0.943)	72.9	**0.001**	0.726 (0.583-0.869)	45.0	**0.007**
IPL	Center	0.614 (0.499-0.729)	25.7	**<0.001**	0.503 (0.350-0.657)	17.3	**<0.001**
	S1	0.858 (0.782-0.934)	63.3	**0.001**	0.852 (0.762-0.943)	46.5	**0.01**
	S2	0.867 (0.791-0.942)	71.3	**0.04**	0.803 (0.694-0.913)	46.2	**0.004**
	I1	0.908 (0.844-0.971)	80.5	0.28	0.923 (0.849-0.998)	80.5	0.68
	I2	0.905 (0.840-0.970)	80.6	0.36	0.847 (0.738-0.956)	63.5	0.07
	N1	0.871 (0.797-0.944)	55.0	**0.004**	0.856 (0.765-0.947)	43.0	**0.005**
	N2	0.839 (0.756-0.923)	70.0	**0.008**	0.741 (0.603-0.878)	47.0	**0.001**
	T1	0.854 (0.770-0.937)	71.0	**0.03**	0.821 (0.692-0.950)	62.0	**0.04**
	T2	0.844 (0.762-0.927)	71.8	**0.02**	0.748 (0.613-0.882)	47.3	**0.002**
	Average Outer	0.888 (0.817-0.960)	70.8	0.05	0.902 (0.829-0.975)	55.0	0.07
	Minimal Outer	0.938 (0.890-0.985)	82.9	Ref	0.938 (0.883-0.994)	77.0	Ref
	Average Inner	0.873 (0.798-0.949)	75.8	0.07	0.816 (0.696-0.936)	57.0	**0.02**
	Minimal Inner	0.888 (0.822-0.955)	77.4	0.15	0.807 (0.690-0.923)	55.9	**0.01**

[a] Delong test.

OCT, optical coherence tomography; AUC, area under the receiver operating characteristic curve; CI, confidence interval; S1, superior outer; S2, superior inner; I1, inferior outer; I2, inferior inner; N1, nasal outer; N2 nasal inner; T1, temporal outer; T2, temporal inner; RNFL, retinal nerve

Journal Pre-proof

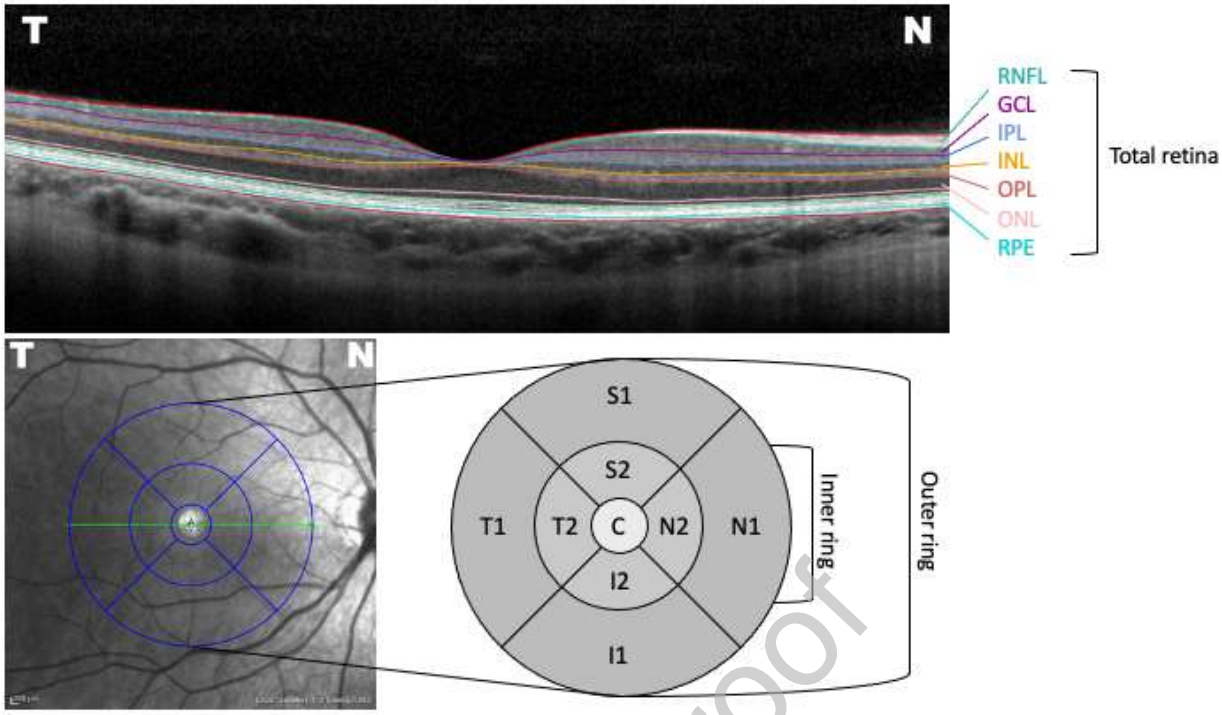

Figure 1. Macular retinal segmentation and the layout of Early Treatment Diabetic Retinopathy Study (ETDRS) grid. Using the automatic segmentation software of Spectralis OCT, thickness of the total retina, retinal nerve fiber layer (RNFL), ganglion cell layer (GCL), inner plexiform layer (IPL), inner nuclear layer (INL), outer plexiform layer (OPL), outer nuclear layer (ONL), and retinal pigmented epithelium (RPE) layer were obtained. The ETDRS grid was applied to each retinal sublayer. Thickness in center (C), superior outer (S1), superior inner (S2), inferior outer (I1), inferior inner (I2), nasal outer (N1), nasal inner (N2), temporal outer (T1), and temporal inner (T2) sectors were measured. The minimal value and average value of outer ring (S1, I1, N1, T1) and inner ring (S2, I2, N2, T2) area in each sublayer were also calculated.

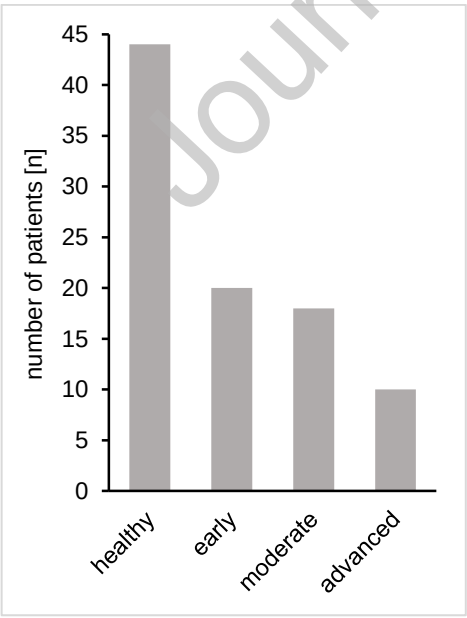

Figure 2. Number of healthy and glaucoma patients with corresponding disease stages in the glaucoma group.

Journal Pre-proof

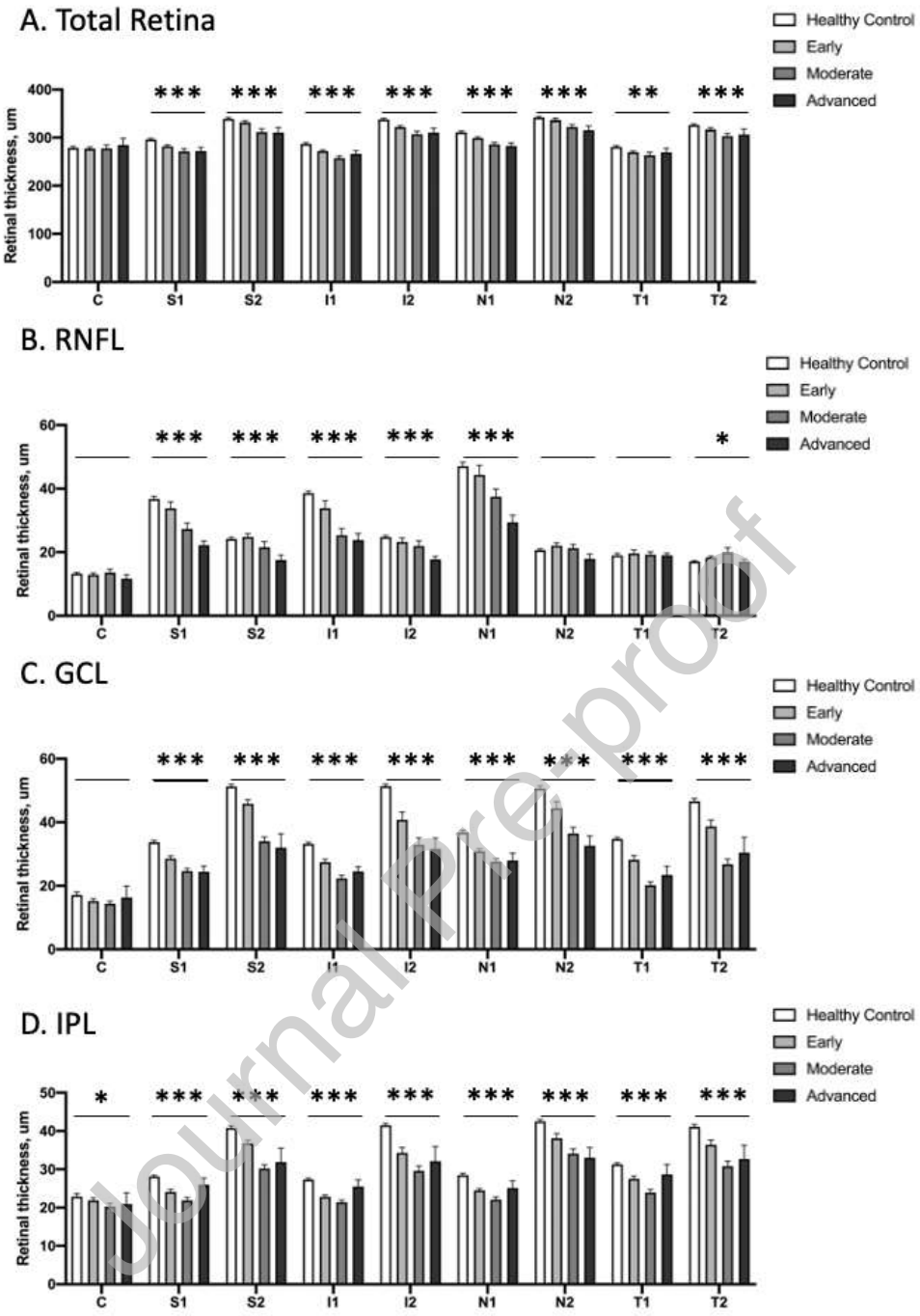

Figure 3. Thickness distribution for the total retina (A) , RNFL (B) , GCL (C) , and IPL (D) in the 9 sectors of ETDRS grid. Mann-Whitney U test showed significant difference in several sectors (*, $p<0.05$, **, $p<0.01$, ***, $p<0.001$).

C, center sector; S1, superior outer sector; S2, superior inner sector; I1, inferior outer sector; I2, inferior inner sector; N1, nasal outer sector; N2, nasal inner sector; T1, temporal outer sector; T2, temporal inner sector; RNFL, retinal nerve fiber layer; GCL, ganglion cell layer; IPL, inner plexiform layer. ETDRS, Early Treatment Diabetic Retinopathy Study.

Journal Pre-proof

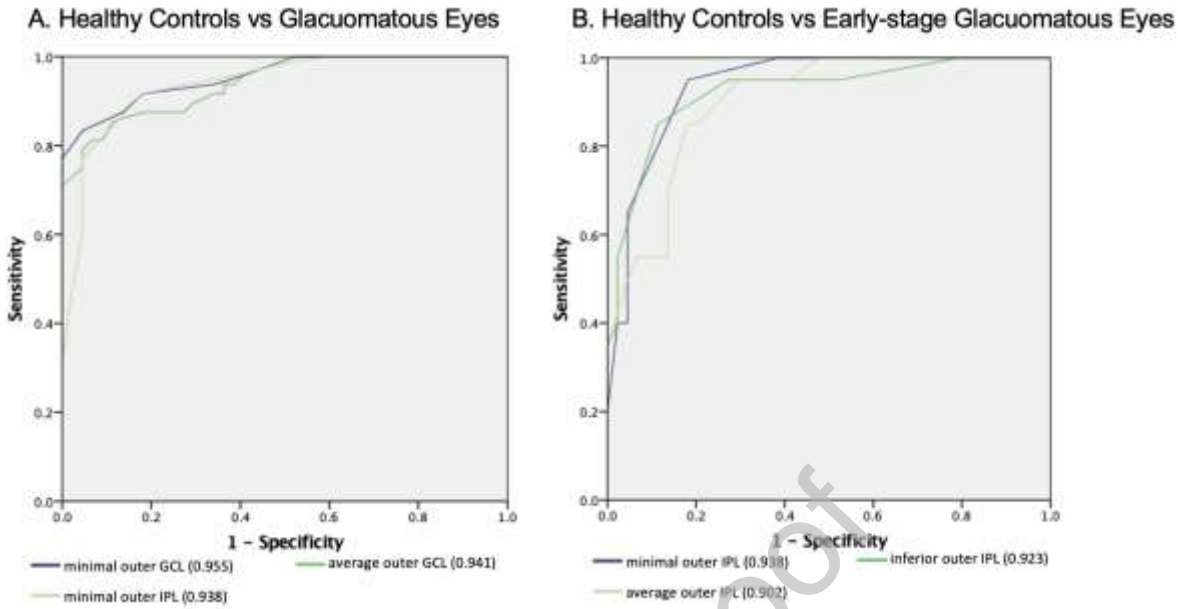

Figure 4. The corresponding receiver operating characteristic curves and AUC values for the OCT parameters with the largest AUC values to discriminate (A) healthy controls and glaucomatous eyes, (B) healthy controls and early-stage glaucomatous eyes.

OCT, optical coherence tomography; AUC, area under the receiver operating characteristic curve; GCL, ganglion cell layer; IPL, inner plexiform layer.

Journal Pre-proof